

# Supporting Information

## **Electroreduction of N<sub>2</sub> and CO<sub>2</sub> to urea via Pd-assisted hydrogenation on MOF-derived CeO<sub>2</sub> nanosheets**

Xiaoyue Chen<sup>1</sup>, Jia Liang<sup>2</sup>, Guangmin Ren<sup>1</sup>, Zhan Zhao<sup>1</sup> and Xiangchao Meng<sup>1\*</sup>

*<sup>1</sup>Key Laboratory of Marine Chemistry Theory and Technology (Ministry of Education), College of Chemistry & Chemical Engineering, Ocean University of China, Qingdao, Shandong, 266100, China.*

*<sup>2</sup>Guangxi Key Laboratory of Electrochemical Energy Materials, School of Chemistry and Chemical Engineering, Guangxi University, 100 Daxue Road, Nanning 530004, China.*

\* Corresponding author. Email: mengxiangchao@ouc.edu.cn

## Experimental section

### Chemicals

1,2,4,5-Benzenetetracarboxylic acid ( $C_{10}H_6O_8$ , BTA, 98%), Cerium nitrate ( $Ce(NO_3)_3 \cdot 6H_2O$ , 99.95%), Palladium chloride ( $PdCl_2$ , AR), Sodium hypochlorite solution ( $NaClO$ , AR) and Sodium nitroferrocyanide dihydrate ( $Na_2[Fe(NO)(CN)_5 \cdot 2H_2O$ , AR) were purchased from Shanghai Aladdin Biochemical Technology Co., Ltd. Sodium hydroxide ( $NaOH$ , AR) and Anhydrous ethanol ( $C_2H_5OH$ , AR) were supplied by Sinopharm Chemical Reagent Co., Ltd.

### Characterizations

X-ray diffraction (XRD, Rigaku Miniflex 600 Japan, Cu K $\alpha$  radiation, scanned range of 5-90°) was used to identify the crystal structure of all prepared catalysts. Scanning electron microscopy (SEM, Czech TESCANA MIRA LMS) and transmission electron microscopy (TEM, JEM-2100PLUS) were utilized to investigate the morphology of all samples. X-ray photoelectron spectroscopy (XPS) data were collected by using Thermo Scientific K-Alpha (USA) monochromatized Al K $\alpha$  cathode source of 75-150 W under ultrahigh vacuum. Thermogravimetric analysis (TGA, Switzerland Mettler TGA/DSC1) was used to analyze the thermal behavior of the prepared nanocomposites. N<sub>2</sub> Temperature Programmed Desorption (N<sub>2</sub>-TPD) was used to test the adsorption capacity of nitrogen on the catalyst surface by means of a chemisorption analyzer (VDsorb-91i, VODO) at a heating rate of 10 °C/min from room temperature to 450 °C. In *situ* Raman measurements were performed in a Renishaw inVia Raman microscope equipped with 532 nm laser in a modified flow cell. The working electrode was a

prepared Pd<sub>0.5</sub>-CeO<sub>2</sub>/C catalyst, the reference electrode was an Ag/AgCl electrode, and the counter electrode was a Pt wire electrode. In-situ Raman spectral data collection was performed at open-circuit potential and potentials ranging from -0.45 V to -0.65 V vs. RHE.

### **Electrochemical measurements**

Electrochemical tests were performed in an H-type electrolytic cell separated using Nafion 117 membranes. Linear scanning voltammetry (LSV) tests were first performed in Ar-saturated and CO<sub>2</sub>+N<sub>2</sub>-saturated 0.1 M KHCO<sub>3</sub> solution at a scan rate of 5 mV s<sup>-1</sup>, respectively, to determine the potential windows for the C-N coupling reaction. The prepared catalysts were loaded on carbon paper (reaction area: 0.5 x 0.5 cm<sup>2</sup>) as working electrode, graphite rod and Ag/AgCl (saturated KCl electrolyte) as counter electrode and reference electrode respectively. The catalyst ink for the working electrode was prepared by dispersing 5 mg of catalyst in a mixed solution of 20 µL of Nafion (0.5 wt%), 490 µL of ethanol, and 490 µL of water and sonicated for 30 min. A mass loading of 0.2 mg cm<sup>-2</sup> was used for electrochemical studies. All experiments were carried out at room temperature (25 °C). In order to remove impurities such as NO<sub>x</sub> from the inlet gas, high purity N<sub>2</sub> (99.999% purity) and CO<sub>2</sub> (99.99% purity) were pre-purified by means of a saturator filled with 0.05 M NaOH and a saturator filled with 0.05 M H<sub>2</sub>SO<sub>4</sub> solution to remove any possible contaminants. The potentials were converted to reversible hydrogen electrode (RHE) scales by the following equation:

$$E(\text{vs. RHE}) = E(\text{vs. Ag/AgCl}) + 0.197 + 0.0591 * \text{pH} \quad (2.1)$$

### **Determination of urea concentration by diacetyl monoxime method**

Urea concentration was determined by the diacetyl monoxime method<sup>1</sup>. 5 g of diacetyl monoxime (DAMO) and 100 mg of thiosemicarbazone (TSC) were dissolved in distilled water and diluted to 1000 mL, which was recorded as DAMO-TSC solution. Then 100 mL of concentrated phosphoric acid was mixed with 300 mL of concentrated phosphoric acid and 600 mL of distilled water, and 100 mg of FeCl<sub>3</sub> was dissolved in the above solution, which was recorded as acid-iron solution. Usually, 1 mL of sample solution was removed from the cathode chamber. Then, 1 mL of DAMO-TSC solution and 2 mL of acid-iron solution were added to 1 mL of sample solution. Next, the mixed solution was heated to 100 °C and held at this temperature for 15 min. When the solution was cooled to 25 °C, UV-VIS absorption spectra were collected at wavelength 525 nm. The concentration-absorbance curves were calibrated with standard urea solutions of series concentrations. The fitted curves showed a good linear relationship between the absorbance values and urea concentration by three independent calibration tests.

The urea yield rate was calculated by the equation:

$$\text{Urea yield rate} = \frac{C \times V}{t \times m} \quad (2.2)$$

The Faradic efficiency (FE) was calculated by the equation:

$$FE = \frac{6 \times F \times c \times V}{60.06 \times Q} \quad (2.3)$$

where  $c$  ( $\mu\text{g mL}^{-1}$ ) is the measured urea concentration,  $V$  (mL) is the volume of the electrolyte,  $t$  (h) is the reduction time, and  $m$  (mg) is the catalyst loading.  $F$  (96500 C mol<sup>-1</sup>) is the Faradic constant, and  $Q$  (C) is the amount of applied electricity.

### **Determination of NO<sub>3</sub><sup>-</sup>**

0.1 mL of 1 M HCl and 10  $\mu$ L of 0.8 wt% C<sub>7</sub>H<sub>6</sub>O<sub>3</sub> solution were sequentially added to 5 mL of electrolyte solution to be tested. After uniform mixing, the absorption spectra in the wavelength range of 200-300 nm were recorded using a Persee TU-1901 dual beam UV-visible spectrophotometer, and the absorbance at 220 and 275 nm were recorded respectively,  $A_{\text{NO}_3^-} = A_{220\text{nm}} - 2A_{275\text{nm}}$ .

### **Determination of NO<sub>2</sub><sup>-</sup>**

First, 0.2 g of C<sub>12</sub>H<sub>14</sub>N<sub>2</sub>·2HCl, 4.0 g of C<sub>6</sub>H<sub>8</sub>N<sub>2</sub>O<sub>2</sub>S, and 10 mL of H<sub>3</sub>PO<sub>4</sub> ( $\rho=1.685$  g mL<sup>-1</sup>) were added to 50 mL of deionized water as a color developer. Next, 0.1 mL of the color developer was added to 5 mL of the electrolyte solution to be tested and mixed thoroughly. The mixed solution was allowed to stand at room temperature for 20 min, and the absorption spectra in the wavelength range of 400 ~ 700 nm were recorded using a Persee TU-1901 dual-beam UV-visible spectrophotometer. Subsequently, the concentration of NO<sub>2</sub><sup>-</sup> was determined by absorbance at 540 nm.

### **Computational Details**

DFT calculations were performed using the Vienna Ab initio Simulation Package (VASP). The modified Perdew-Burke-Ernzerhof exchange-correlation density functional (PBE) was used to describe the exchange-correlation energy under the generalized gradient approximation (GGA). A planar fluctuation energy cutoff of 420 eV was chosen. We created 3  $\times$  3  $\times$  3 supercells to simulate Pd-CeO<sub>2</sub>/C surfaces. Atomic positions were fully relaxed until the maximum energy difference and residual force on the atoms converged to 10<sup>-5</sup> eV and 0.03 eV  $\text{\AA}^{-1}$  eV, respectively, and 15  $\text{\AA}$

thick vacuum layer was used to avoid interactions between the upper and lower surfaces.

The calculation formula was as follows:

$$\Delta G = \Delta E + \Delta E_{ZPE} - T\Delta S \quad (2.4)$$

where  $\Delta E$  was obtained from DFT energy calculations,  $\Delta E_{ZPE}$  and  $T\Delta S$  for the adsorbed species were calculated from vibrational analyses, and thermodynamic corrections for the gas molecules were obtained from standard databases.

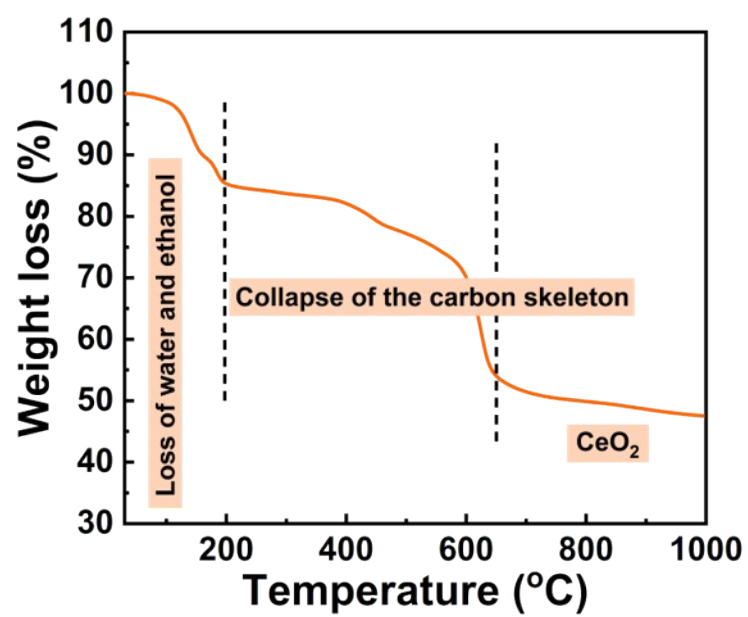


**Figure S1.** TGA curves of Ce-MOF.

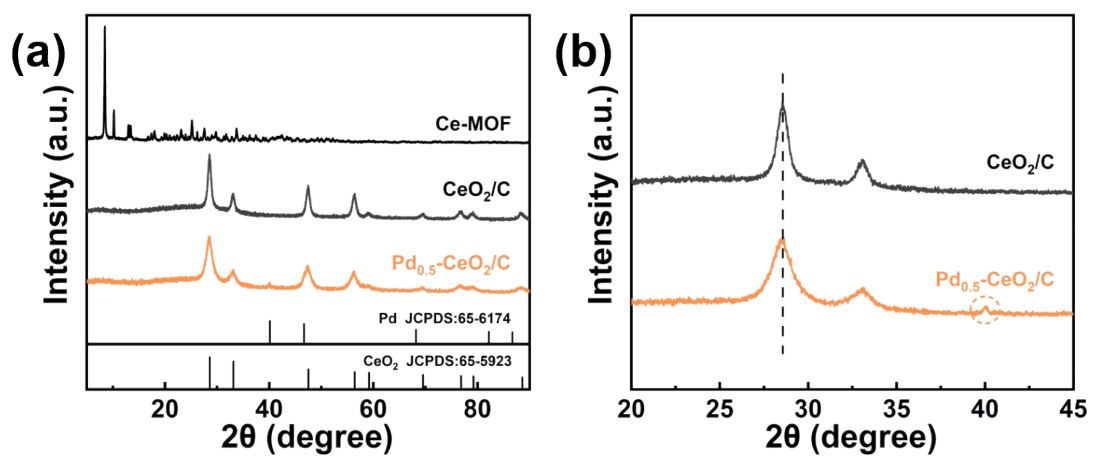


**Figure S2.** XRD pattern of (a) Ce-MOF, CeO<sub>2</sub>/C and Pd<sub>0.5</sub>-CeO<sub>2</sub>/C; (b) Partially enlarged XRD diffraction pattern of CeO<sub>2</sub>/C and Pd<sub>0.5</sub>-CeO<sub>2</sub>/C.



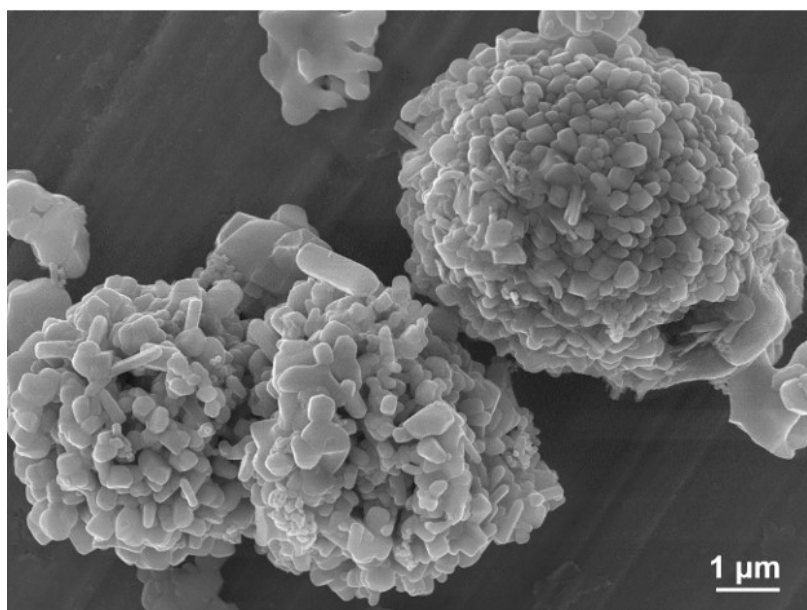


**Figure S3.** SEM images of Ce-BTC MOF.

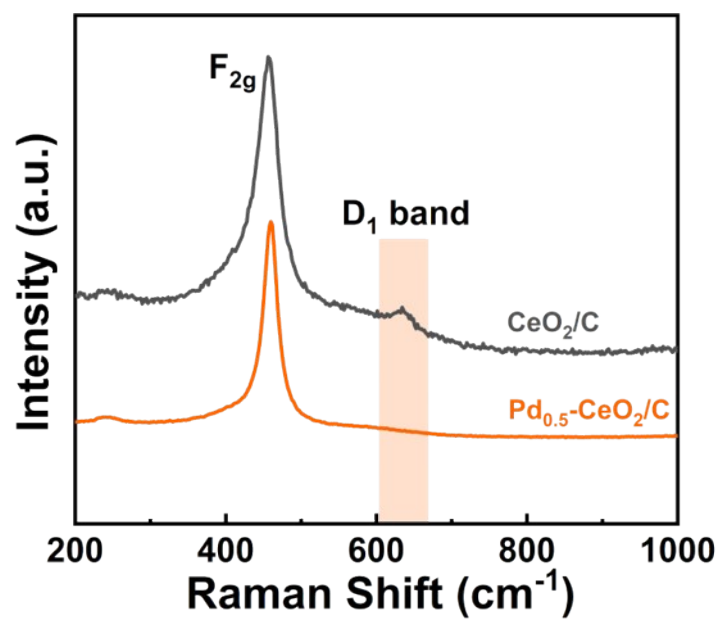


**Figure S4.** Raman spectra of CeO<sub>2</sub>/C and Pd<sub>0.5</sub>-CeO<sub>2</sub>/C.

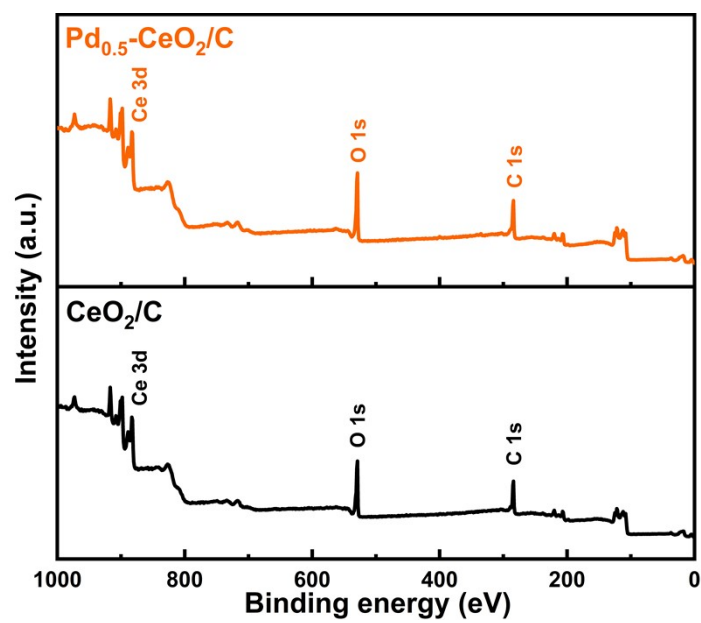


**Figure S5.** XPS spectra of  $\text{Pd}_{0.5}\text{-CeO}_2/\text{C}$  and  $\text{CeO}_2/\text{C}$ : Survey.

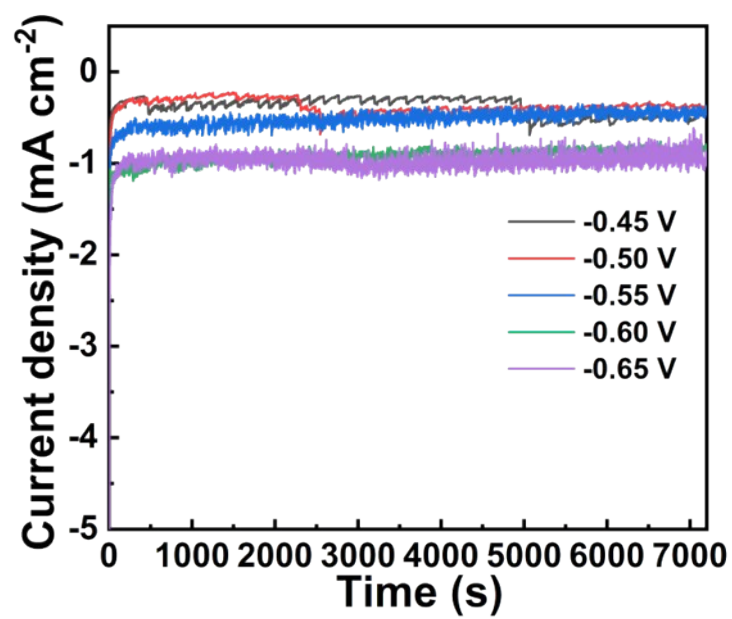


**Figure S6.** The chronamperometric curves of Pd<sub>0.5</sub>-CeO<sub>2</sub>/C at various potentials for 2 h in N<sub>2</sub> and CO<sub>2</sub>-saturated 0.1 M KHCO<sub>3</sub> solution.

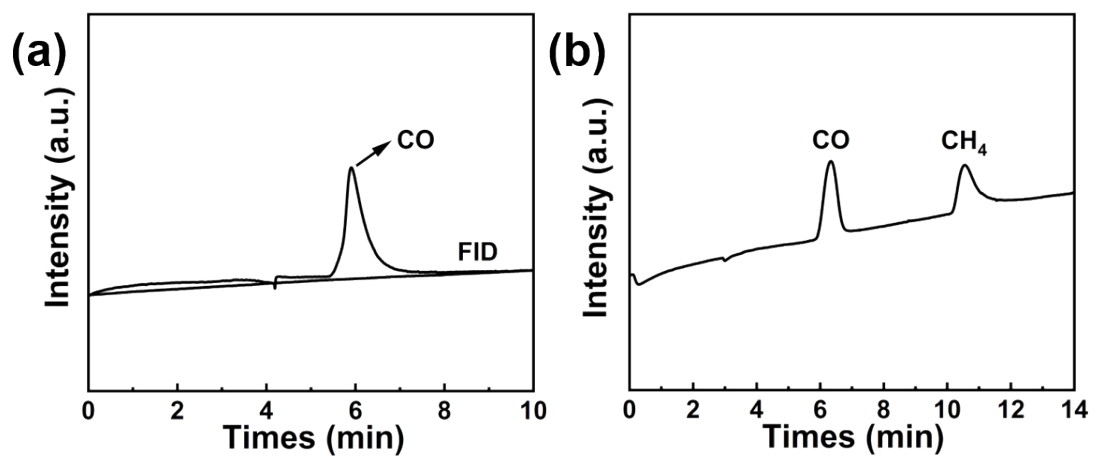


**Figure S7.** (a) Gas chromatogram after 2 h of electrocatalytic C-N coupling reaction;  
(b) Standard gas chromatograms for CO and CH<sub>4</sub>.

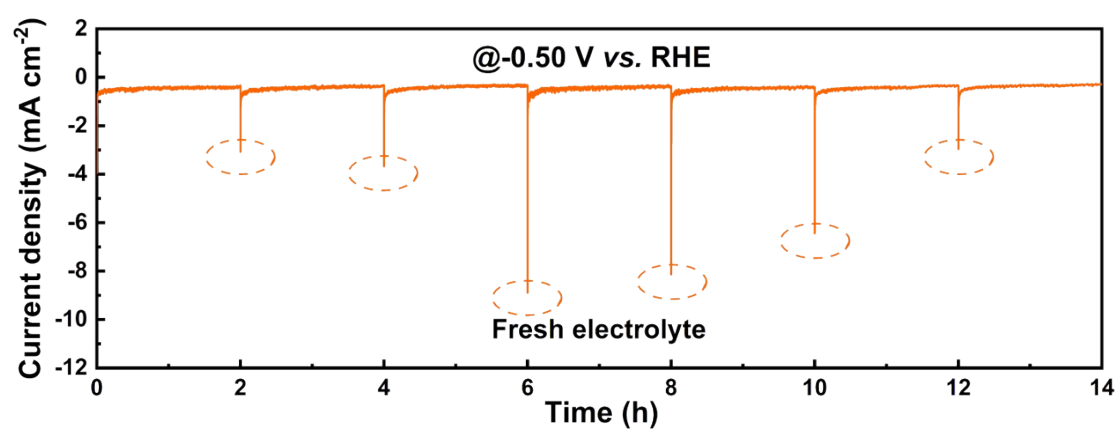


**Figure S8.** Time-dependent current density curves at -0.50 V vs. RHE during recycling tests.

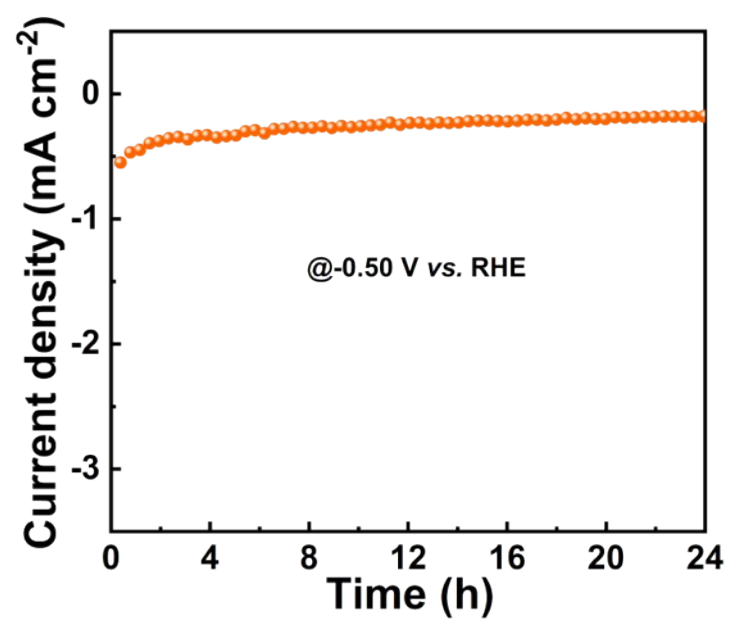


**Figure S9.** Time-dependent current density curves of 24 h at -0.50 V vs. RHE.

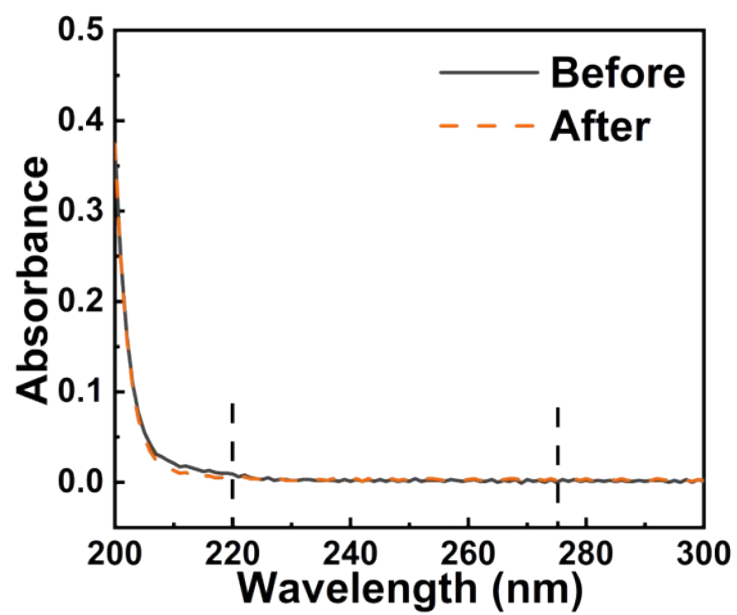


**Figure S10.** UV-Vis absorbance spectra of  $\text{NO}_3^-$  before and after bubbling  $\text{CO}_2 + \text{N}_2$  for 30 minutes.



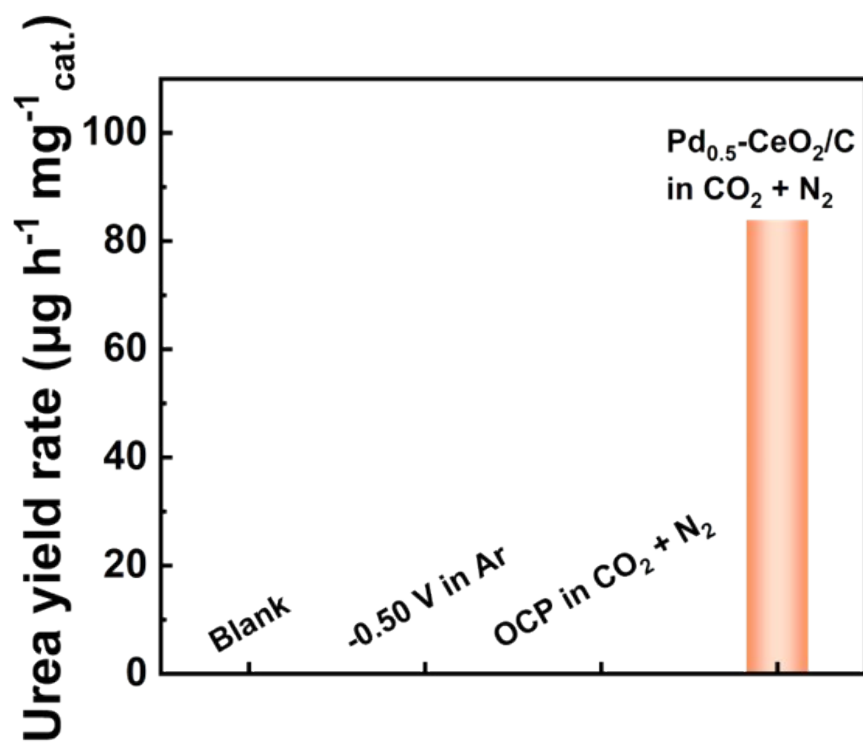


**Figure S11.** Urea yield rates under different test conditions.

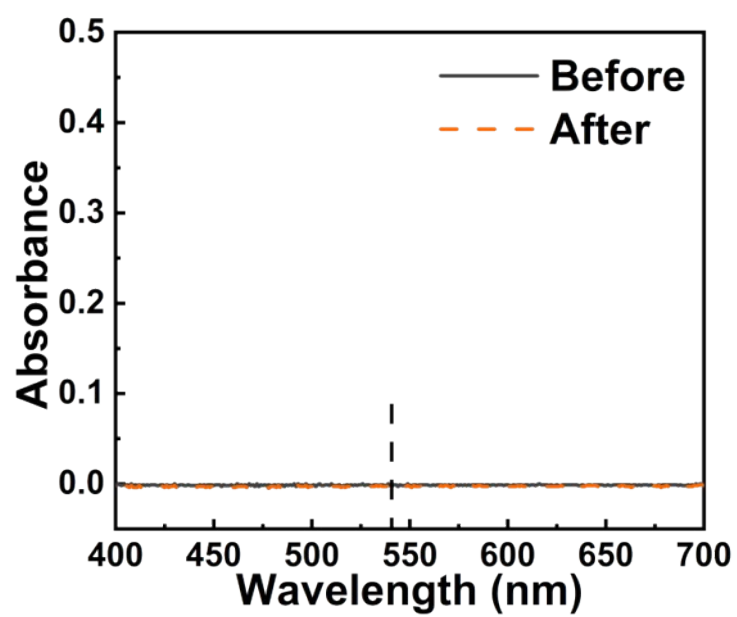


**Figure S12.** UV-Vis absorbance spectra of  $\text{NO}_2^-$  before and after electrolytic  $\text{CO}_2 + \text{N}_2$  reduction for 2 h.

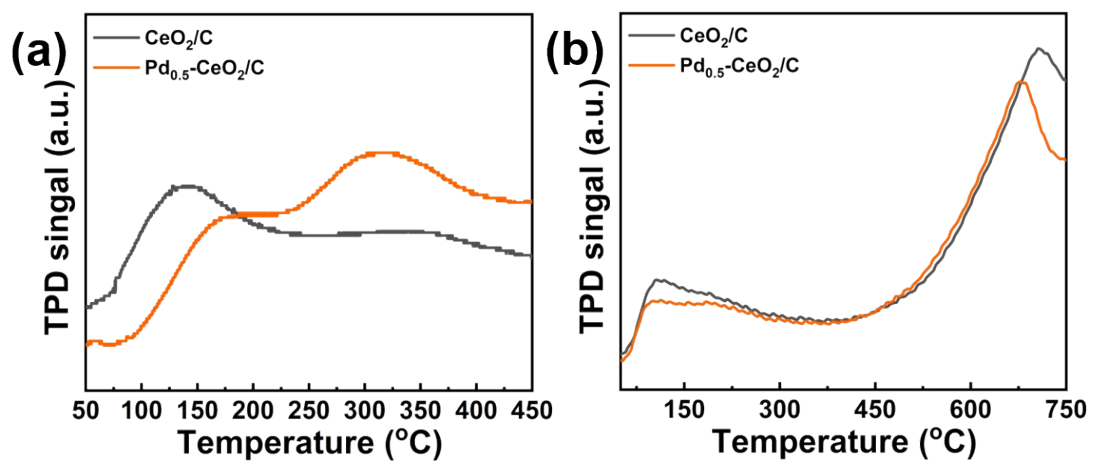


**Figure S13.** (a)  $\text{N}_2$ -TPD spectra and (b)  $\text{CO}_2$ -TPD spectra of  $\text{Pd}_{0.5}\text{-CeO}_2/\text{C}$ , and  $\text{CeO}_2/\text{C}$ .

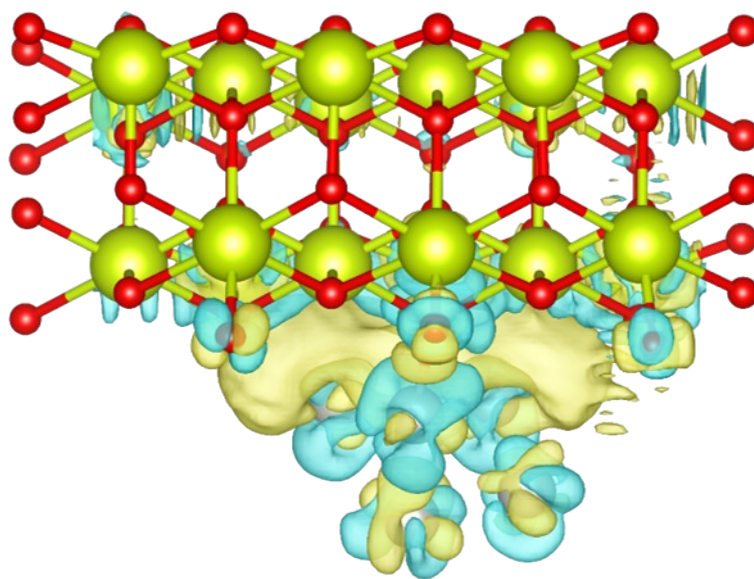


**Figure S14.** Bader charge density difference for Pd<sub>0.5</sub>-CeO<sub>2</sub>/C.

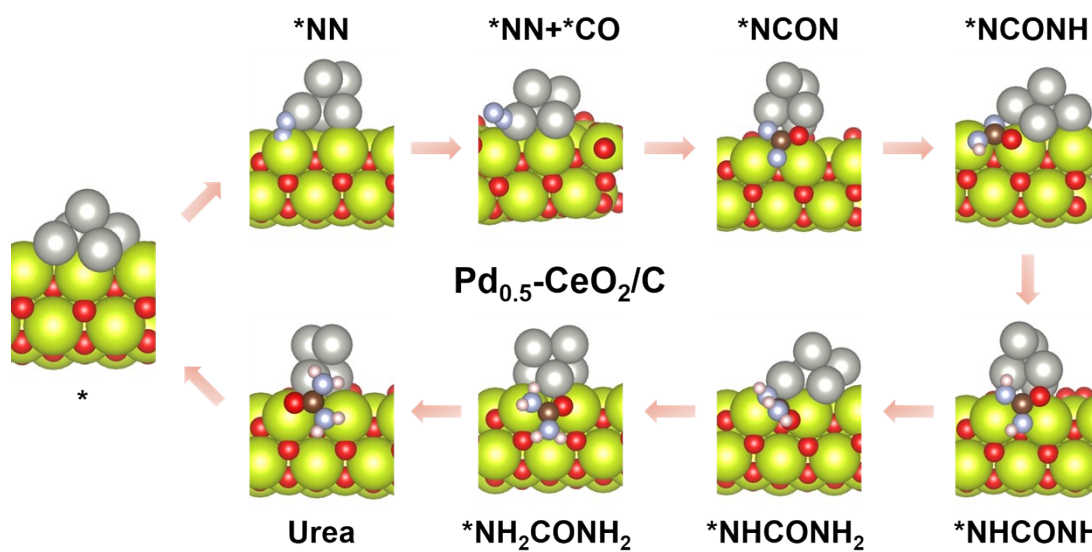


**Figure S15.** Schematic representation of urea synthesis using  $\text{Pd}_{0.5}\text{-CeO}_2/\text{C}$  nanosheet.

**Table S1.** Comparison of Pd<sub>0.5</sub>-CeO<sub>2</sub>/C and other catalysts for electrocatalytic C-N coupling activity for the synthesis of urea under ambient conditions using N<sub>2</sub> and CO<sub>2</sub> as sources.

Catalyst	Urea Yield Rate	Faradic Efficiency (%)	N-source	Reference
Pd <sub>0.5</sub> -CeO <sub>2</sub> /C	83.89 μg h <sup>-1</sup> mg <sup>-1</sup> <sub>cat.</sub>	11.92	N <sub>2</sub>	This work
Fe-N-C	0.156 μmol mg <sup>-1</sup> h <sup>-1</sup>	2.13	N <sub>2</sub>	2
FePc	0.357 μmol h <sup>-1</sup> mg <sup>-1</sup> <sub>cat.</sub>	14.36	N <sub>2</sub>	3
Bi <sub>2</sub> S <sub>3</sub> /N-RGO	4.4 μmol mg <sup>-1</sup> h <sup>-1</sup>	7.5	N <sub>2</sub>	4
PdCu/TiO <sub>2</sub>	3.36 μmol h <sup>-1</sup> mg <sup>-1</sup>	8.92	N <sub>2</sub>	5
MoP(101)	12.4 μg h <sup>-1</sup> mg <sup>-1</sup>	36.5	N <sub>2</sub>	6
V <sub>N</sub> -Cu <sub>3</sub> N-300	81 μg h <sup>-1</sup> cm <sup>-2</sup>	28.7	N <sub>2</sub>	7
CuPc NTs	143.47 μg h <sup>-1</sup> mg <sup>-1</sup> <sub>cat.</sub>	12.99	N <sub>2</sub>	8
CuWO <sub>4</sub>	98.5 ± 3.2 μg h <sup>-1</sup> mg <sup>-1</sup> <sub>cat.</sub>	70.1 ± 2.4	NO <sub>3</sub> <sup>-</sup>	9

## References

1. Mhammed Rahmatullah and T. R. C. Boyde, Improvements in the determination of urea using diacetyl monoxime; methods with and without deproteinisation, *Clin. Chim. Acta*, 1980, **107**, 3-9.
2. Y. Huang, K. Luo, W. Yang, X. Chen, M. Wang, L. Shi, L. Zhu, X. Mao, X. Ji, T. Xu, H. Zhu and X. Wang, Urea Electrosynthesis in Microbial Electrolysis Cells Using Low-cost Fe–N–C for Simultaneous N<sub>2</sub> and CO<sub>2</sub> Reduction, *Industrial & Engineering Chemistry Research*, 2023, **62**, 13450-13457.
3. S. R. Waghela, A. Adalder, K. Mitra and U. K. Ghorai, Electrocatalytic Urea Synthesis via C–N Coupling Over Fe-Based Catalyst, *ChemCatChem*, 2024, **17**, e202401565.
4. P. Xing, S. Wei, Y. Zhang, X. Chen, L. Dai and Y. Wang, Electrochemical Co-reduction of N<sub>2</sub> and CO<sub>2</sub> to Urea Using Bi<sub>2</sub>S<sub>3</sub> Nanorods Anchored to N-Doped Reduced Graphene Oxide, *ACS Appl. Mater. Interfaces*, 2023, **15**, 22101-22111.
5. C. Chen, X. Zhu, X. Wen, Y. Zhou, L. Zhou, H. Li, L. Tao, Q. Li, S. Du, T. Liu, D. Yan, C. Xie, Y. Zou, Y. Wang, R. Chen, J. Huo, Y. Li, J. Cheng, H. Su, X. Zhao, W. Cheng, Q. Liu, H. Lin, J. Luo, J. Chen, M. Dong, K. Cheng, C. Li and S. Wang, Coupling N<sub>2</sub> and CO<sub>2</sub> in H<sub>2</sub>O to synthesize urea under ambient conditions, *Nat. Chem.*, 2020, **12**, 717-724.
6. D. Jiao, Y. Dong, X. Cui, Q. Cai, C. R. Cabrera, J. Zhao and Z. Chen, Boosting the efficiency of urea synthesis via cooperative electroreduction of N<sub>2</sub> and CO<sub>2</sub> on MoP, *J. Mater. Chem. A*, 2023, **11**, 232-240.
7. Z. Lv, S. Zhou, L. Zhao, Z. Liu, J. Liu, W. Xu, L. Wang and J. Lai, Coactivation of Multiphase Reactants for the Electrosynthesis of Urea, *Adv. Energy Mater.*, 2023, **13**, 2300946.
8. J. Mukherjee, S. Paul, A. Adalder, S. Kapse, R. Thapa, S. Mandal, B. Ghorai, S. Sarkar and U. K. Ghorai, Understanding the Site-Selective Electrocatalytic Co-Reduction Mechanism for Green Urea Synthesis Using Copper Phthalocyanine Nanotubes, *Adv. Funct. Mater.*, 2022, **32**, 2200882.
9. Y. Zhao, Y. Ding, W. Li, C. Liu, Y. Li, Z. Zhao, Y. Shan, F. Li, L. Sun and F. Li, Efficient urea electrosynthesis from carbon dioxide and nitrate via alternating Cu–W bimetallic C–N coupling sites, *Nat. Commun.*, 2023, **14**, 4491.